A Tribological and Electrochemical Study of Protic Ionic Liquid and Bentonite Particles Used as Lubricating Additives in Water-Based Lubricants

Victor Velho de Castro[1] · Leonardo Moreira dos Santos[2] · Leonardo Marasca Antonini[1] ·
Roberto Moreira Schroeder[1] · Silvana Mattedi[3] · Klester S. Souza[4] · Marcelo Barbalho Pereira[5] ·
Cleber Rodrigo de Lima Lessa[6] · Sandra Einloft[2] · Carlos Alexandre dos Santos[2] · Célia de Fraga Malfatti[1]

Abstract

The objective of this work is to evaluate the wear and corrosion behaviours of different formulations of water-based lubricants containing protic ionic liquid (PIL) and bentonite particle additions. Carbon-steel samples were investigated in the normalized and quenched-tempered conditions. Wear tests and corrosion tests using potentiondynamic polarization curves were performed in the presence of different lubricant solutions (PIL 3 wt% + deionized water, with 0.05 wt% and 0.1 wt% bentonite particle additions). Wear scar surfaces were analysed by scanning electron microscopy (SEM), energy-dispersive spectroscopy (EDS), and Raman techniques. Unexpected electrochemical effects caused by the bentonite addition promoted the formation of a thick oxide film (Fe_3O_4) in the quenched-tempered steel during the wear test, which mitigated the wear in the presence of a minimum amount of this particle in the formulation.

Keywords Bentonite · Protic ionic liquids · Tribology · Corrosion · Carbon steels

✉ Victor Velho de Castro
  victor.castro@ufrgs.br

1 Department of Metallurgy, Corrosion Research Laboratory
   (LAPEC), Federal University of Rio Grande do Sul
   (UFRGS), Porto Alegre, Rio Grande do Sul, Brazil

2 School of Technology, Pontifical Catholic University of Rio
   Grande do Sul (PUCRS), Porto Alegre, Rio Grande do Sul,
   Brazil

3 Department of Chemical Engineering, Laboratory of Applied
   Thermodynamics, Federal University of Bahia (UFBA),
   Salvador, Bahia, Brazil

4 Department of Inorganic Chemistry, Bioanalytical
   Laboratory,, Federal University of Rio Grande do Sul
   (UFRGS), Porto Alegre, Rio Grande do Sul, Brazil

5 Institute of Physics, Laser & Optics Group, Federal
   University of Rio Grande do Sul (UFRGS), Porto Alegre,
   Rio Grande do Sul, Brazil

6 Federal Institute of Science and Technology of Rio Grande
   do Sul (IFRS), Caxias do Sul, Rio Grande do Sul, Brazil

1 Introduction

In numerous industrial applications such as metal forming, machining, oil and gas extraction, assembly processes, lubricants are essential to ensure high performance of the processes. Usually, hydrocarbon-based lubricants are utilized. However, the tendency to replace fossil-lubricants with water-based lubricants is increasing. Nonetheless, these lubricants exhibit poor performance compared to petroleum-based lubricants and accelerate the corrosive process in steels [1]. An alternative to improve the work performance of water-based lubricants is to use specific additives as active surface (or interface) molecules, which could be solid nanoparticles, ionic liquids, or biobased oils [2].

Among the particles used as a lubricant additive, graphite is a solid lubricant widely used as an additive in lubricants. [27–29]. However, graphite has a very noble electrochemical potential, which can induce galvanic corrosion when in contact with steels in water-based lubricants. Therefore, the search for lubricating particles that have potential lubricating capacity (equivalent to graphite) but do not accelerate the corrosive process is justified. In this context of search for solid additives that do not induce corrosive processes

in metallic materials, bentonite appears as an alternative to replace graphite as a lubricating particle.

A bentonite (smectite) is a clay composed predominantly of the clay mineral montmorillonite. It is formed by layers consisting of two tetrahedral sheets and an octahedral sheet. The space between the layers is occupied by hydrated exchangeable cations, for example, Na^+, Al^{3+}, Mg^{2+}, and Fe^{2+}, which are charge compensators [3]. These particles can have several applications, such as sand binders, iron ore pellets, and ceramic shell additives [4]. In addition, it is common practice to use bentonite suspensions as a lubricant in pipe jacking [5]. The ability to exchange cations and the variation of the basal distance when exposed to moisture (expansion when exposed to water and contraction on drying) are known characteristics of montmorillonite type bentonites [6]. Many studies have analysed the phenomena in the interaction between steels and bentonite [7–9]. These studies reported that changes in clay in contact with Fe depend on many parameters such as the water/solid ratio, iron/clay mass, pH, temperature, time, and mineralogy [10].

Ionic liquids (ILs) have shown potential for numerous applications, including energy storage devices, catalysis, biomass processing, pharmaceuticals, and CO_2 capture [11–14]. ILs are liquid organic salts composed of an anion and a cation, with at least one proton and capable of forming hydrogen bonds. The hydrogen bond (HB) formation occurs in ILs when the composed cations possess hydrogen atoms, and the anions have appropriate H-atom acceptors. Ionic liquids can be divided into two categories: aprotic ionic liquids and protic ionic liquids. They are produced by transferring protons from a Bronsted acid to a Bronsted base. Aprotic solvents cannot donate hydrogen bonds, and protic ones can donate the hydrogen bond (dissociable H +), that is, they can donate H + (protons) [15]. Since the beginning of the century, the use of ILs as lubricants has been studied [16].

One of the most studied groups of IL is the aprotic ionic liquids (APIL) [17]. Most APILs contain halogen elements such as fluorine or chlorine, which can easily form hydrofluoric acid or hydrochloric acid when exposed to the moisture atmosphere, and then corrode metal parts. APILs are also very expensive because of their complicated synthesis route [18].

Protic ionic liquids (PILs), however, which are another subset of IL, have a wide range of properties such as high viscosity, high thermal and electronic conductivity, non-flammability, and low toxicity in addition to being good solvents. [19]. These properties, combined with the easy synthetic route, low cost, and toxicity, make PILs a suitable alternative to APILs in lubrication [20]. PILs can also be used as additives [21, 22]. A series of polymer-based ionic liquids with a flexible and electron-rich polymeric chain attached to the cation have been designed as lubricants for steel–steel systems. Surface characterizations

and molecular dynamics simulations show super lubricity results from the robust lubricating film immediately formed at the steel surface due to the rapid adsorption of FA-IL ions via multiple sites [23]. The wear reduction ability of bis(2-hydroxyethyl) ammonium oleate PIL in a glycerol aqueous lubricating fluid was analysed [24]. The tribo-tests were performed using a ruby–steel friction pair acting in reciprocation mode. It was hypothesized that the formation of the adsorption layer and metal soap was responsible for reducing the wear and COF. Ten PILs based on the combination of methylimidazolium ([MIMH]), 4-picolinium ([4-picH]), pyridinium ([PyrH]), 1,8-diazabicyclo[5.4.0]-undec-7-ene-8-ium ([DBUH]), and tetramethylguanidinium ([TMGH]) cations with hydrogen sulphate ([HSO₄]) and mesylate ([MeSO3]) anions were tested as additives in polyethylene glycol (PEG200) to lubricate steel/silicon and silicon/silicon contacts [25]. The best additive was [4-picH][HSO4], which adsorbed on the Si surface, and reduced wear by up to 15 times. Three oleate-based PILs were used as lubricants for aluminium, aiming to apply them in metal-forming processes [26]. Oleate-based PILs maintained a low COF value, with the formation of uniform tribofilms that promoted the wear reduction down to 98% compared to the dry condition.

ILs have been studied as lubricating additives and can be used in association with lubricating particles. In the work by Avilés et al. [30], the tribological behaviour of halogen-free ionic liquid PILs was analysed. The results showed that the coefficient of friction (COF) decreased throughout the test due to the evaporation of water from the emulsion. Other works have analysed the behaviour of ILs as additives in lubricants containing water [31, 32]. A recent work carried out by our research group has investigated water-based lubricant formulations containing m-2HEAOL and talc additions [33]. It was demonstrated that the adsorption capacity of the PIL on the metallic surface of the steels increased the lubricity of the formulation when compared to commercial additives. Furthermore, electrochemical tests showed that PILs are efficient corrosion inhibitors [34–36] in addition to having low toxicity [37]. In this context, the study of other lubricating particles is justified. Thus, the objective of this work was to analyse, for the first time, the effect of adding bentonite particles and a PIL (m-2HEAOL) in water-based lubricants, on the tribological and electrochemical responses. The lubricity of the proposed formulations was tested in a ball-on-plate tribometer, using AISI/SAE 1010 and AISI/SAE 1045 steels as the metallic substrate. Lubrication and wear mechanisms were investigated. Corrosion inhibition capacities were determined at the concentrations studied through electrochemical tests of potentiodynamic polarization curves.

2 Experimental Procedure

2.1 Lubricants

In the present study, both PILs and bentonite particles were considered as additives. The formulations composed of deionized water (DI water) and additives were considered as lubricants. The synthesis methodology was based on scientific papers of Iglesias et al. [38] and Mattedi et al. [39]. The characterization of m-2HEAOL was performed and previously published in another scientific paper developed by our research group [26]. The water-based lubricants were obtained by an aqueous solution with the addition of 3 wt% of m-2HEAOL (Table 1), utilized as the additive at the concentration of 3 wt%. For this purpose, the lubricants were subjected to mechanical agitation for 5 h and then remained at rest for 24 h. The investigated lubricants are shown in Table 1. To change the corrosivity of the formulations and study the tribological consequences, sodium nitrite ($NaNO_2$) was added to the formulations. The results of the eroded volumes of formulations without this additive and formulations with $NaNO_2$ were compared.

Particles of Nanoclay (hydrophilic bentonite, Sigma-Aldrich, also known as montmorillonite) were added at concentrations of 0 wt%, 0.05 wt%, and 0.1 wt%. The Bentonite Brookfield viscosity was measured by a Brookfield Viscometer (RVDV-I Prime, spindle SC4-21, 50 rpm and 100 rpm) at 23 °C. The pH was evaluated using a pH meter (Model Dm-22, Digimed). Three pH measurements were performed for each formulation.

Particle size distribution (PSD) measurements of the bentonite particles were performed in water solution, after 15 min in an ultrasonic bath, using the Laser Diffraction Particle Size Analyzer (Model 1180, Cilas). X-ray diffraction analysis (XRD) of the bentonite particles was carried in a Shimadzu X-ray Diffractometer (Model XRD 7000, Shimadzu). Copper k alpha radiation, 40 kV, 20 mA, angles ranging from 2° to 60°, and step size of 1°/s were used for the analyses. Lubricants with 3 wt% of commercial additive (based on vegetable esters, free of chlorine, nitrites, phenols, and boron) and bentonite particles were used as a reference in the wear tests. This commercial water-based lubricant was also used as a preliminary test to evaluate the use of bentonite particles as a lubricant additive in conjunction with a known additive already on the market. Due to the corrosivity of water in the steel alloys studied, it was not possible to carry out tests on formulations containing only water without corrosion inhibitor additives. Generalized corrosion occurred on the surface of the samples, which prevented the analysis of the wear tracks formed during the tribological test.
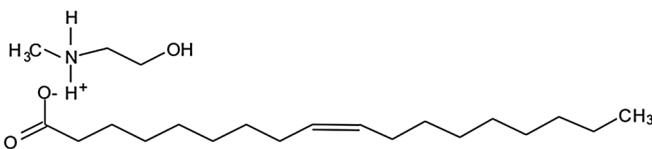
2.2 Specimens

To investigate the lubrication and corrosion inhibition performances of the lubricants, tests were carried out in carbon steels with different chemical compositions and microstructures: AISI/SAE 1010 and AISI/SAE 1045 steels. The AISI/SAE 1010 steel was normalized at 800 °C, and the AISI/SAE 1045 steel was austenitized at 850 °C, quenched in oil, and tempered at 300 °C. These materials were chosen because they are used in numerous metalworking applications, such as rolling, forging, stamping, and cutting, where lubricated conditions are usually required. All specimens were ground with silicon carbide sandpapers (# 80, #120, #320, #400, #600, #800, #1200), followed by polishing with an alumina solution (0.1 µm). The average surface roughness (Ra) and absolute surface roughness (Rz) were measured after the sample preparation using a portable linear surface roughness tester (Model Surftest SJ-410, Mitutoyo).

2.3 Wettability Tests

Wettability tests in the steel surfaces were performed. Samples were placed in immersion for 1 h, and after that tests were conducted. Contact angle measurements were performed using the sessile drop method and an apparatus developed by the Corrosion Research Laboratory (LAPEC) of the Federal University of Rio Grande do Sul (Porto Alegre, Brazil). The deionized water drop was observed through a low-magnification lens and the contact angle measured in Surftens 4.5 software.

Table 1 PILs used in the studied lubricants. Adapted from Vega et al. [26]

PIL	Structure
m-2HEAOl N-methyl-2-hydroxyethylammonium oleate	

2.4 Electrochemical Tests

Potentiodynamic polarization curves (PPC) were run only in the lubricant solution containing the higher bentonite concentration (0.1 wt%) in both carbon steels, using the Autolab potentiostat (Model PGSTAT302N, Metrohm). The PPC measurements were obtained in the voltage range of − 800 mV (in the cathodic direction) and + 1000 mV (in the anodic direction), corresponding to the value for the E_{OCP} with a scan rate of 1 mV/s. The cell was composed of a saturated calomel reference electrode, a salt bridge (KCl and agar–agar solution), and the carbon steels as working electrodes. Before the test, the working electrode was immersed in the solution for 30 min to attain a steady-state open-circuit potential (with variations lower than 5 mV/s). A light microscope (Model Lab. 1, Zeiss Axio) was used after the test for analysing the sample surfaces. Corrosion rates were determined according to the ASTM G 102 standard method [40]. Data were collected by electrochemical software NOVA ver2.1.4®. The E_{corr} and I_{corr} were estimated by Tafel extrapolation method.

2.5 Wear Tests

For evaluating the behaviour of the different lubricants, immersed wear tests were conducted according to ASTM G133 [41] using a ball-on-plate tribometer (Universal Micro Tribometer, CETR UMT). During the tests, the kinetic COF was determined. The parameters used in all wear tests were 1 N normal load (maximum Hertz stress of approximately 700 MPa) [42], frequency of 2 Hz, 5 mm stroke, and 36 m sliding distance (test duration of 1 h). An Yttria-Stabilized Zirconia sphere (Grade 10, Macea) with 4.8 mm diameter, 1510 HV microhardness, and 0.020 µm roughness (Ra) was used as the counterbody material. The parameters were chosen in order to promote tribofilm formation during the tests. All tests were carried out in triplicate.

The disc volume loss (Vm) and the COF in both the disc and sphere were determined as recommended by the ASTM G133 standard method [41]. All wear tracks were analysed using a field emission gun—scanning electron microscope (FEG-SEM Model 50, Inspect). The wear tracks were also analysed by Raman spectroscopy in a laser Raman spectrometer (Model DXR, Horibam LabRamHr—laser excitation wavelength of 532 nm) and in a micro-Raman single-spot analysis and mapping microscope (Model alpha300, Oxford Instruments—laser excitation wavelength of 632.8 nm). Before analysis, the samples were cleaned and dried with cold air.

3 Results and Discussion

3.1 Lubricant and Specimen Characterization

The studied lubricants are presented in Table 2. All lubricants presented a viscosity of approximately 30 mPa.s, conducting a limit lubrication regime ($\lambda < 1$) [43, 44]. The viscosity tests did not detect significant changes in the lubricants containing bentonite particles in the proportions of 0.05 wt% and 0.1 wt%. The pH values of the lubricants were within standard deviation and, therefore, there were no significant differences between the measured pH values between the two bentonite concentrations. It is known that due to the physicochemical properties of the m-2HEAOL molecule, the pH of these formulations can be high. In addition, the addition of particles further increased the alkalinity of these lubricants, with pH values close to 9.0. The pH measured in an aqueous solution of bentonite, at levels higher than those in this work, indicated values of 8.0 [4].

Figure 1A shows the granulometric distribution (normal distribution) and the SEM image of the bentonite microparticles in a humid environment. It is known that clays can increase the basal distance by the intercalation of water molecules [6] among other chemical species, leading to variation in their dimensions. Therefore, the average dimensions that the lubricant particles would have in the lubricant formulations were measured. As for the particle size, 90% of them have dimensions up to 2.58 µm, 50% of the particles have up to 1.26 µm, and 10% have up to 0.52 µm. The average diameter of the particles was approximately 1.43 µm. Previous works show that particles with dimensions greater than 0.5 µm and with spherical morphology (Fig. 1B) are not the most suitable for application as lubricants, as they tend to not produce a stable suspension due to the tendency of particles in suspension to precipitate and because they make it difficult to fill surface peaks and valleys due to their high dimension [45, 46]. However, the measured values

Table 2 Composition, viscosity, and pH of the studied lubricants

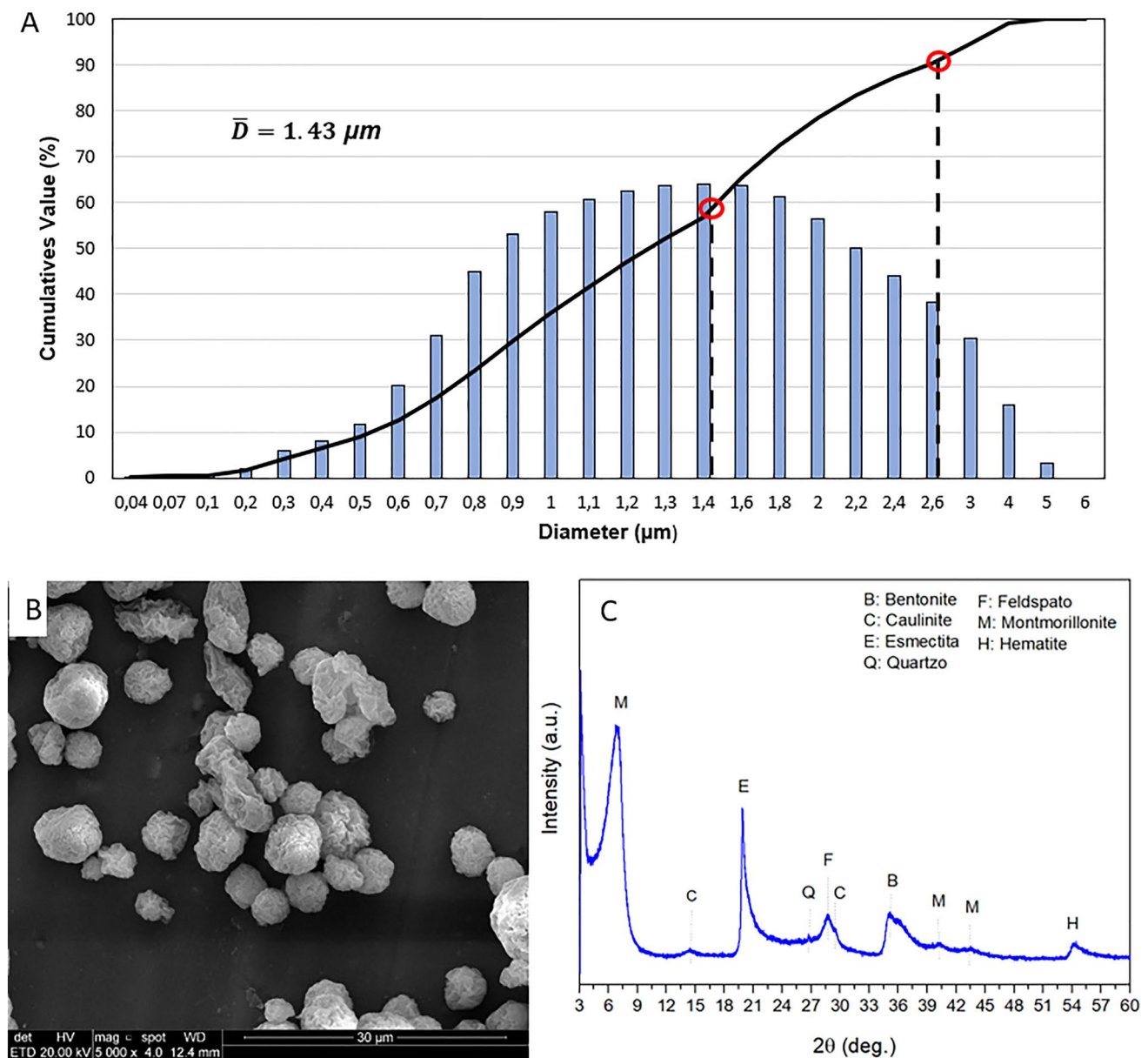| Sample	Composition	Viscosity 100 RPM (mPa.s)	pH
m-2HEAOL_WP	H_2O + 3 wt% of m-2HEAOL	30 (0.5)	8.0 (0.5)
m-2HEAOL_ BT _0.1	H_2O + 3 wt% of m-2HEAOL + 0.1 wt% of bentonite	30 (0.5)	8.7 (0.5)
m-2HEAOL_ BT _0.05	H_2O + 3 wt% of m-2HEAOL + 0.05 wt% bentonite	30 (0.5)	9.1 (0.5)

Fig. 1 Characterization of bentonite particles. **A** Particle size distribution; **B** SEM showing the morphology of the particles; **C** XRD of particles

of roughness Rz (Table 2) were between 2.1 and 2.3 μm. Therefore, the particles of bentonite would be effective in filling in the surface irregularities, thus, reducing the wear and slip resistance. In addition, with the size distribution determined and mentioned above, a precipitation of part of the bentonite on the surface of the track and the steel during the wear tests would be expected, which would allow the filling of irregularities and the interaction of the particle and the surface of the steels.

From the XRD analysis of the particles used as the additive (Fig. 1C), the presence of bentonite and smectite (montmorillonite) was detected. Traces of quartz, hematite, and kaolinite were also detected [3, 47–50]. No contaminants

that could alter the electrochemical and lubricity behaviour of this additive were detected.

Wettability tests were performed, and a water droplet contact angle of $80° \pm 4.5°$ for SAE 1010 steels and $88° \pm 4.5°$ for SAE 1045 steels were determined. The metallic substrates presented a wettability of $32° \pm 1.0°$ for the SAE 1010 and $42° \pm 3.4°$ for the SAE 1045. Thus, there was a significant increase in the hydrophobicity of the surfaces of the samples compared to the substrates. The observed surface hydrophobicity can be attributed to the adsorption of IL molecules on the steel, which may be related to the amphiphilic character of m-2HEAOL [34]. The alkyl chains of the anion molecules behave in a hydrophobic manner,

while the carboxylate anion, which has a polar character, behaves in a hydrophilic manner, as does the cationic fraction. However, this adsorbed layer behaves in a hydrophobic manner compared to the substrate, with a difference in the contact angle of up to 40° [51]. When adding bentonite in the lubricant containing m-2HEAOL, a marked difference between the contact angle measurements is not evidenced (around 42°) because the PIL molecule already performs sufficient interactions with water, minimizing the effect of montmorilonite, since the content added is low, not affecting the wettability measurements.

The chemical composition, hardness, and surface roughness of the samples of both substrates are shown in Table 2. The quenching heat treatments followed by tempering resulted in a tempered martensitic microstructure in the AISI/SAE 1045 steel samples with high hardness (approximately 531 HV ≈ 51 HRC), while the AISI/SAE 1010 samples showed a ferritic-pearlitic matrix (with an approximate hardness of 130 HV ≈ 72 HRB). According to the microstructures obtained and the hardness values measured, AISI/SAE 1045 steel must have high mechanical strength and good toughness, while AISI/SAE 1010 steel must be ductile and not very resistant. The microstructure obtained after the thermal treatment was like that found in a previous work of our research group [33]. The surface roughness after the sanding and polishing process was similar on both substrates, as expected. The standard deviation values are represented in parentheses.

3.2 Electrochemical Tests

To analyse the behaviour of the lubricants in aqueous media, polarization curves were run on samples of both steel alloys, on lubricants containing m-2HEAOL with and without 0.1 wt% bentonite particles. Assays in deionized water without particles (Water_WP) and containing 0.1 wt% particles (Water_BT_0.1) were also performed.

The results are shown in Fig. 2. Analysing the SAE 1010 steel curves, with the Water_BT_0.1, electrolyte showed an abrupt increase in the current density approximately at the potential of 250 mV$_{SCE}$, indicating a greater acceleration in the corrosive process above this potential generated by BT particles (TC = 4.20×10^{-4} mm/year). This behaviour was not found in the test containing only water (Water_WP), which showed a constant increase in the current density and TC = 3.70×10^{-4} mm/year. The curves with m-2HEAOL, from potentials close to 250 mV$_{SCE}$ with and without the presence of montmorillonite particles, showed a pseudo-passivation, probably associated with the adsorption of the PIL [34]. The similar behaviour between these two curves demonstrates the corrosion inhibition capacity of m-2HEAOL on this substrate.
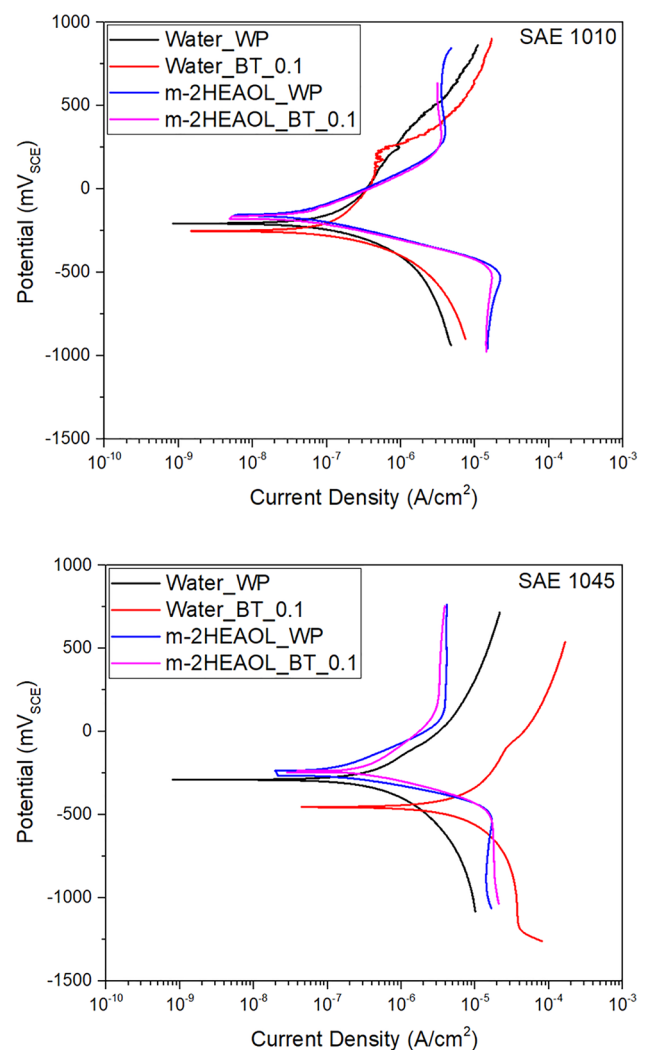

Fig. 2 Comparison of potentiodynamic polarization curves with and without lubricating particles of SAE 1010 and SAE 1045 substrates

The corrosion potentials presented in Table 4 stabilized at -230 mV$_{SCE}$ and -375.5 mV$_{SCE}$ in the tests with the Water_WP and Water_BT_0.1 electrolyte, respectively, indicating an increase in corrosion due to the presence of bentonite. However, in the presence of the PIL, E_{Corr} shifted to nobler potentials between − 155 mV$_{SCE}$ and − 145 mV$_{SCE}$, indicating a better corrosion behaviour in the presence of additives. Corrosion current densities in the tests for this steel remained at levels close to 10^{-2} μA/cm^2. The m-2HEAOL_WP lubricant tests showed slightly lower values, with current density of 3.29×10^{-2} μA/cm^2. This was reflected in the corrosion rate (2.89×10^{-4} mm/year).

The tests in water for the quenched and tempered SAE 1045 steel showed a higher reactivity than for the SAE 1010 steel, taking the corrosion rates to higher values, where Water_WP presented a corrosion rate of 15.8×10^{-4} mm/year. As seen in Fig. 3, after the electrochemical test, the
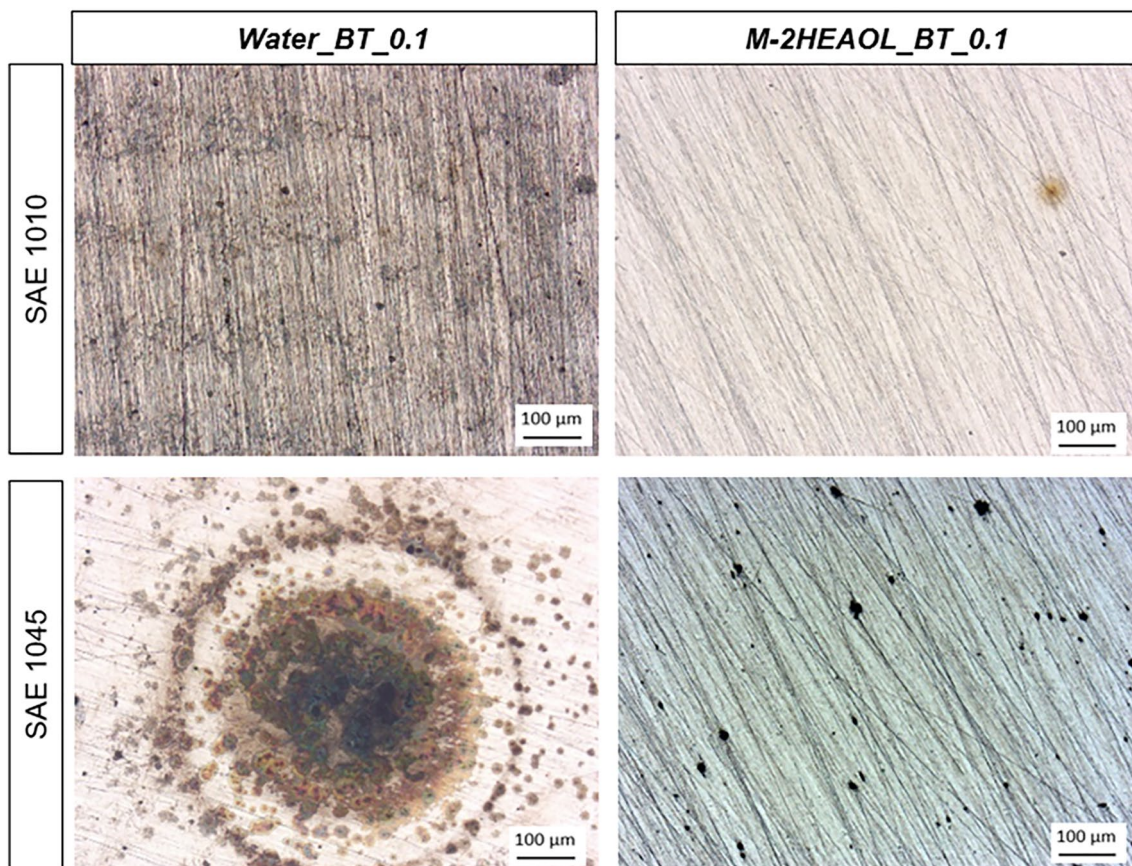
Fig. 3 Surface of samples after electrochemical testing

SAE 1045 steel sample in the Water_BT_0.1 electrolyte showed pronounced pitting and red corrosion products. It is known that despite some controversy, many researchers indicate that martensite obtained by quenching has a greater tendency to corrode compared to other structures, such as pearlitic and bainitic structures [52], and has the highest corrosion rate among steel microstructures [53]. The polarization curves for SAE 1045 steel in the presence of the Water_BT_0.1 electrolyte (Fig. 3) showed a shift towards higher current densities in relation to the Water_WP electrolyte and a lower noble corrosion potential ($E_{corr} = -462.5$ mV_{SCE} and $I_{Corr} = 2.47 \times 10^{-1}$ $\mu A/cm^2$). Consequently, it has the highest corrosion rate among the systems studied ($CR = 116.5 \times 10^{-4}$ mm/year). Water_BT_0.1 presented a pH 8.8, and a higher pH was probably not the cause of the greater corrosion observed. XRD analysis, as previously mentioned, indicates that the increase in the corrosive process was not caused by contamination by corrosive substances from the bentonite particles.

Jeannin et al. [54] demonstrated that the main interaction effect between the steel surface and the different analysed particles was observed with the presence of bentonite. The bentonite particles, which coated the electrode, partially blocked contact with the electrolyte, preventing widespread corrosion. However, this favoured localized corrosion, which can develop in the steel through the pores of the mineral layer. On the other hand, it is known that bentonite and smectites could exchange cations with the environment. This property is known as cation exchange and normally favours the exchange of Al^{+3} for Mg^{+2} or Fe^{+2} in tetrahedral sheets [6]. In this context, Gaudin et al. [10] demonstrated that different steel alloys (stainless steels and carbon steels) showed a corrosive process after 6 years in contact with clays. These authors explain that magnetite can form in the region of contact between steel and clay, encouraged by the presence of bentonite, according to reaction (1). The magnetite formed can also be transformed into goethite and lepidocrocite, in addition to amorphous phases, which is in line with the high corrosion rates found in the Water_BT_0.1 electrolyte in the SAE 1045 steel.

$$Fe^{2+} + 2Fe^{3+} + 4H_2O = Fe_3O_4 + 8H^+. \qquad (1)$$
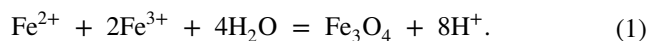
During the steel oxidation process, local acidification occurs on the surface of the material (production of H^+),

which can cause the dissolution of the smectite present in the clay used in this study (Fig. 1) [10, 55].

As demonstrated in Fig. 2, the corrosive effect of the clay was nullified by m-2HEAOL due to the strong adsorption of the functional groups present in the strongly polar molecule of the PIL, as proposed by Schimtzhaus et al. [34]. Therefore, the polarization curves of the m-2HEAOL_WP and m-2HEAOL_BT_0.1 lubricants showed very similar behaviour for both substrates, inhibiting, to a certain extent, the corrosive effect of bentonite. The corrosion rates in the tests in these formulations were lower than in the tests in water with and without particles for both substrates (Table 4).

Furthermore, the results for the polarization curves for both substrates were like those obtained for water-based formulations applying commercial additive and talc particles, performed in a previous study [33]. Thus, the potential of m-2HEAOL as a corrosion inhibitor is confirmed, even in the presence of bentonite particles, which proved to be more corrosive than the talc addition.

3.3 Tribological Tests

3.3.1 Bentonite Wear Tests

To measure the lubricity of bentonite particles, tests were carried out on formulations containing 3 wt% of commercial additive and the proposed concentrations of BT. As shown in Fig. 4, the COF of the tests lubricated with a commercial lubricant was lower than that of the dry test. Tests performed without lubrication showed COF between 0.6 and 0.8 for normalized AISI/SAE 1010 steel and close to 0.4 for quenched and tempered AISI/SAE 1045 steel. The lower hardness and mechanical strength of AISI/SAE 1010 steel, combined with the heterogeneity of the ferritic-pearlitic microstructure, allow for a more severe wear process on this substrate, generating a greater change in the topography within the wear track, which causes greater resistance to the sliding of the counterbody, raising the COF. In AISI/SAE 1045 steel, this change also occurs but with less intensity due to the higher wear resistance of these samples due to the greater hardness and mechanical resistance, in addition to the homogeneity of the martensitic microstructure.

The lubricity of the commercial additive, as expected, reduced the COF to approximately 0.1 and remained stable throughout the test. However, as the measured COF was very
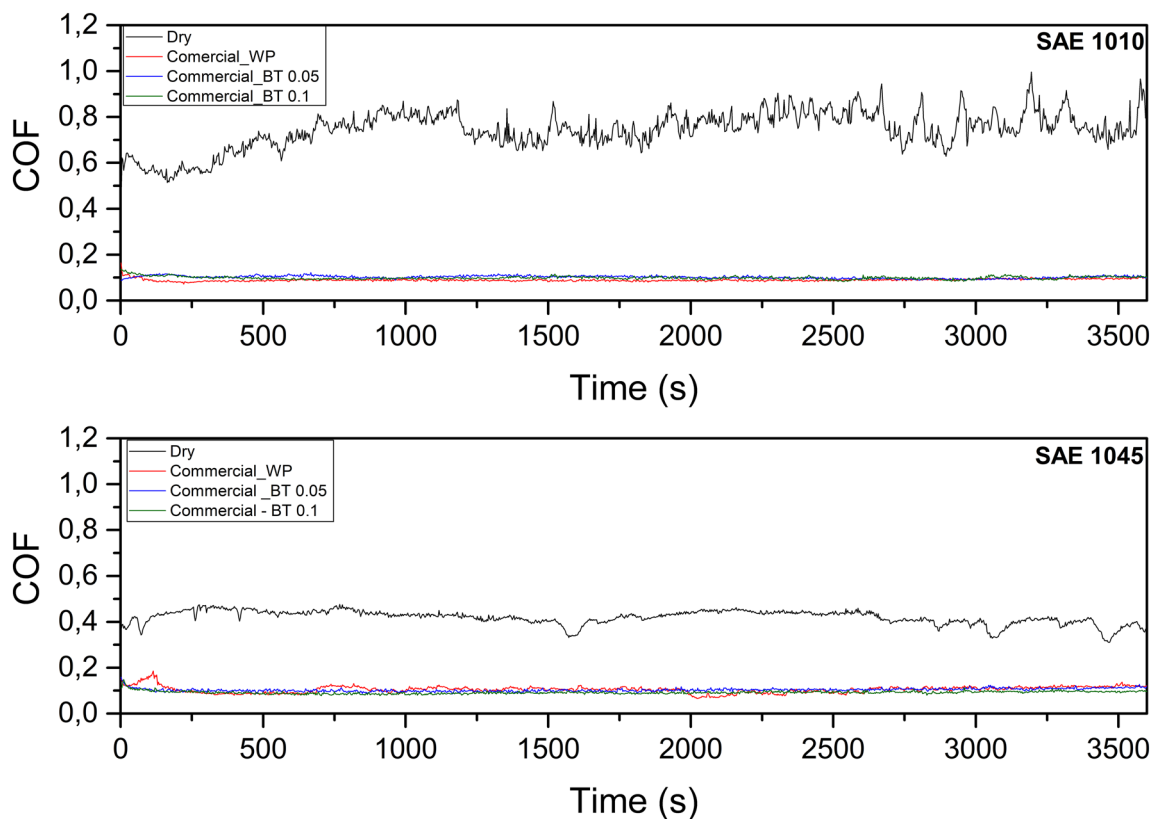

Fig. 4 Surface of samples after electrochemical testing (commercial)

similar for the tests lubricated with commercial additive and bentonite, the effect of the bentonite particles on the reduction of the sliding resistance was not detected.

However, the worn volume of the wear tracks was reduced as the concentration of BT particles was increased, demonstrating the lubricating potential of these particles (Fig. 5). The characteristic roughness length scale of shearing surfaces is smaller than the radius of the nanoparticles, as demonstrated in Fig. 1 and Table 3, settling inside the asperities, and reducing the worn volume [56].

3.3.2 PIL and Bentonite Tribological Tests

Figure 6 presents the coefficients of friction (COF) found in the tribological tests for both steels. The lubricated tests presented lower COFs than the dry tests, demonstrating the lubricity action of the formulations tested in both materials. As previously commented, the limit lubrication regime acted during the tests with all the proposed formulations. It is known that in this lubrication regime, the physicochemical characteristics of the lubricants play a more important role than the viscosity [43, 44]. All lubricated tests showed a COF close to 0.2. This similarity is due to the lubrication mechanism exerted by the PIL, which was possibly predominant because, as mentioned above, it easily adsorbs on the surfaces of the steels. Furthermore, the COF measured for formulations containing m-2HEAOL and bentonite was similar to those for formulations containing commercial additive. This demonstrates the lubricant potential of these formulations [33].

The lubrication mechanism of ionic liquids in the boundary lubrication regime can form strong adsorption films on the friction surfaces due to the polarity of the ILs and lead to a reduction of wear by interaction with the formed surface tribofilm. Longer alkyl chains in IL cations, such as those present in m-2HEAOL molecules, are more likely to form thick films due to Van der Waals forces [14]. It is known that the main mechanism of lubrication of ILs is by adsorption, which is a key factor for lubrication [57, 58]. Two factors determined the improvement in lubricity generated by the PILs: better coverage of the lubricant on the surface of the sample and the strong interaction between the lubricant and the surface of the steel. The best coverage is attributed to the balance of the lubricant's hydrophobic and hydrophilic properties. The balance between these properties is reached when the hydrocarbon chain is introduced into the PIL molecule [59]. The results of Huang et al. [60] indicated a strong adsorption of cations on the steel surface, where they played an important role in the lubricity of the lubricants studied by these authors. In addition, there is a great advantage in the adsorbed layer of the PIL in relation to other existing additives, as the interactions between the tribofilm and the newly worn surface increase the performance of the lubricant. The anionic part of the ionic liquid can be easily adsorbed to positively charged locations on the worn surface of the metal, providing protection against severe wear. Therefore, under

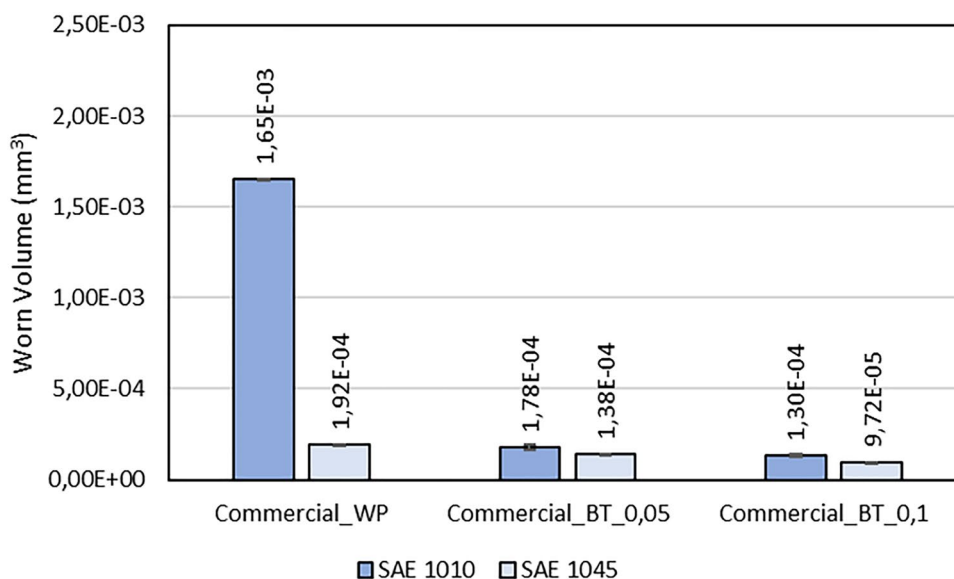**Fig. 5** Worn volumes of samples from both substrates (commercial)

Table 3 Chemical composition of the steel samples

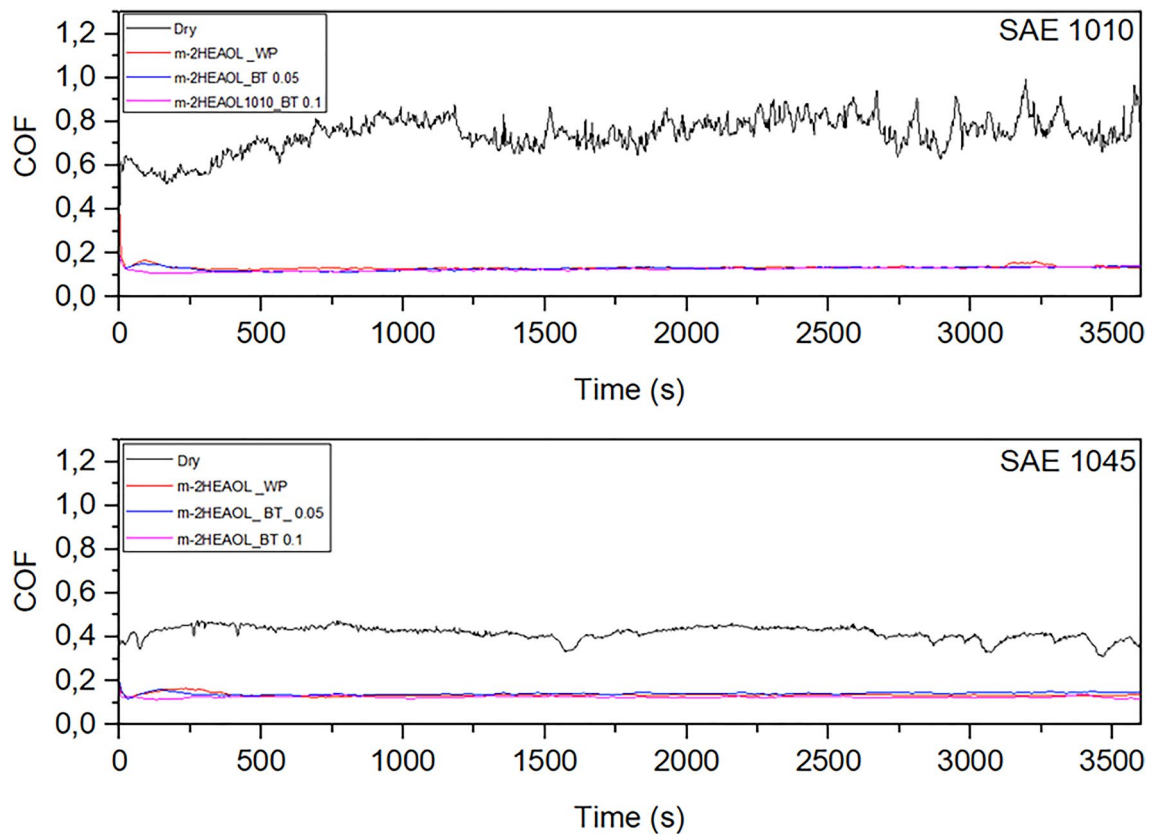| Steel	Fe (%)	C (%)	Si (%)	Mn (%)	P (%)	Hardness (HV)	Ra (µm)	Rz (µm)
SAE 1010	99.30	0.10	0.10	0.40	0.10	130 (20.5)	0.3 (0.1)	2.3 (0.3)
SAE 1045	98.50	0.47	0.15	0.50	0.02	531 (9.0)	0.3 (0.1)	2.1 (0.4)

Fig. 6 Comparison between dry wear test with different lubricant formulations

adverse slip conditions, active elements in ionic liquids can react with the worn surface, forming a reaction lubricating film on the newly worn surface of the sample [61].

This adsorbed layer was detected by Raman spectroscopy (wavelength of 532 nm), as shown in Fig. 5. The characteristic peaks of oxygenated organic compounds, as C=O (670 cm^{-1}) [60], CO (770 cm^{-1}) [61], COC (941–1050 cm^{-1}) [62], in addition to the carbon chain: CC (1062 cm^{-1}, 1251 cm^{-1}) [63, 64], C=C (1555 cm^{-1}) [65], –CH_2– (815 cm^{-1})]. The D and G bands can form during the wear process, resulting in the formation of this structure [62]. This adsorbed layer led to similar low COFs in all lubricated assays (Fig. 7). As demonstrated in a previous paper [33], this adsorbed film gives the m-2HEAOL action a greater capacity to reduce the worn volume of the tracks than the commercial additive when diluted in water with 3 wt%.

Bentonite particles were not detected. The difficulty in finding characteristic peaks of bentonite molecules in lubricants may be associated with the absence of covalent bonds formed between the lubricants and the particles. In this case, the bentonite particles were probably mixed with the lubricants, and a strong surface/particle interaction did not occur.

Figure 8 shows the spheres aspect after the wear test, using optical microscopy. Note the presence of grooves on the surface of the spheres related to microcutting/microplugging wear micromechanisms linked to the abrasive wear process [34]. Figure 9 shows the worn volumes of these counterbodies. Except for the dry test on quenched and tempered AISI/SAE 1045 steel, all worn volumes showed wear below 1.0×10^{-6} mm^3. These results were close to those found in these formulations without particles and with talc particles [33]. Possibly the greater hardness and mechanical resistance of this steel, associated with the thick oxide layer formed in the wear track of this test (Fig. 10), contributed to the greater wear of this sphere, under the specific conditions of this test. Scanning Electron Microscope (SEM) and Energy Dispersive Spectroscopy (EDS) analyses did not detect the presence of Fe adhered to the beads.

As shown in Fig. 10, this thick tribofilm was also formed in the non-lubricated test of AISI/SAE 1010 steel and in the lubricated test of the m-2HEAOL_BT_0.1 formulation. The tribolayers are a result of the tribochemical reaction. These phenomena occurred between the wear track surfaces under the conditions of boundary limit lubrication [63]. The tribolayer formed by oxides and the material of both counterfaces and their oxides are called the mechanically mixed layer [64, 65]. The Raman analysis with wavelength of 632.8 nm (Fig. 10) detected the presence of Fe oxides
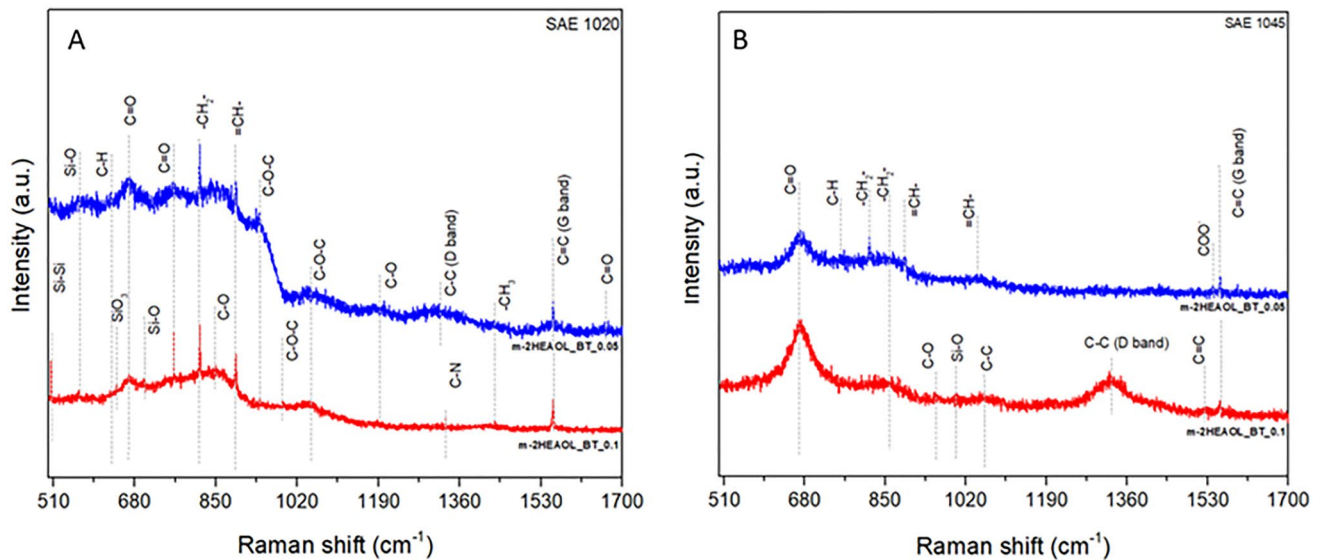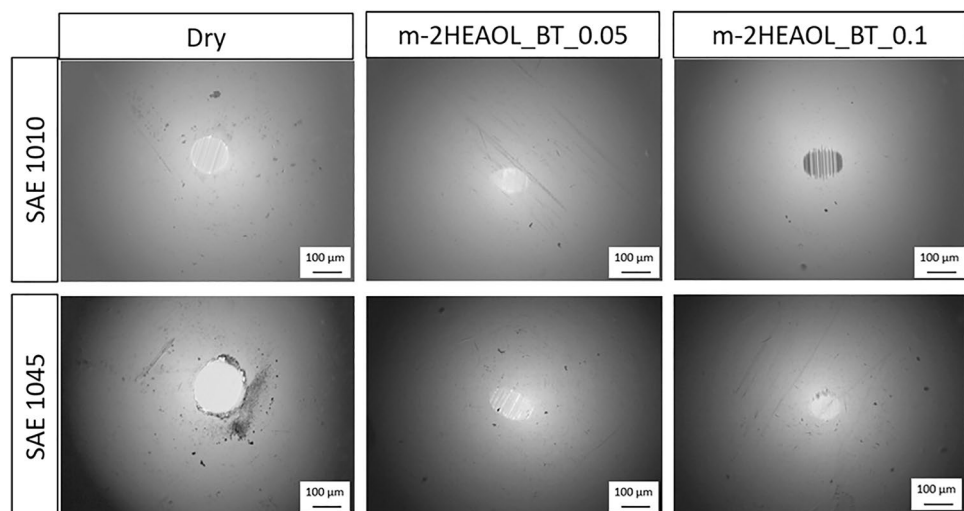
Fig. 7 Analysis by Raman spectroscopy (wavelength of 532 nm) in the wear tracks: **A** normalized AISI/SAE 1010 steel, **B** AISI/SAE 1045 steel quenched and tempered

**Fig. 8** Optical microscopy of the spheres applied in the assays

(α-Fe$_2$O$_3$—hematite and Fe$_3$O$_4$—magnetite) in all analysed tests. They may be formed due to corrosive processes or due to the elevated temperature on the surfaces. Furthermore, the presence of hematite in the wear track is indicative of a tribological system with low wear [66]. These oxides were also found in tests using the PIL in lubricant formulations [67]. In the case of tests without lubrication, these oxides are associated with high temperatures and can be formed by the tribooxidation [68, 69]. The lubrication-free wear process forms a "hot-spot" temperature in the real contact areas [70, 71], promoting the formation of these oxides. The Hertz stresses involved were insufficient to break this layer, which were above the critical thickness [69]. It is known that FeO$_3$ and Fe$_3$O$_4$ are hard and brittle oxides and could

suppress deformation under certain conditions [72]. Thus, these thermal oxides formed a protective layer that prevented the formation of the wear track, as seen in the cross-sectional profile of the tracks (Fig. 11). As the lubricants used in the study are water based, hydrated oxides (as α-FeOOH and γ-FeOOH) can also be associated with peaks at the same wavelength numbers (298, 397, 414, 1322 cm^{-1}) [73, 74].

In the test of AISI/SAE 1045 steel lubricated with m-2HEAOL_BT_0.1, combined with dry wear, frictional temperatures in lubricated wear are much lower and the presence of PIL may limit or prevent oxide film growth [71]. Therefore, the oxide layer formed was thinner, allowing the formation of the wear track (Figs. 10 and 11) and the detection of the worn volume (1.14×10^{-6} mm^3) (Fig. 12).

Fig. 9 Worn ball volume: **A** counterbody for AISI/SAE 1010 steel, **B** counterbody for AISI/SAE 1045 steel
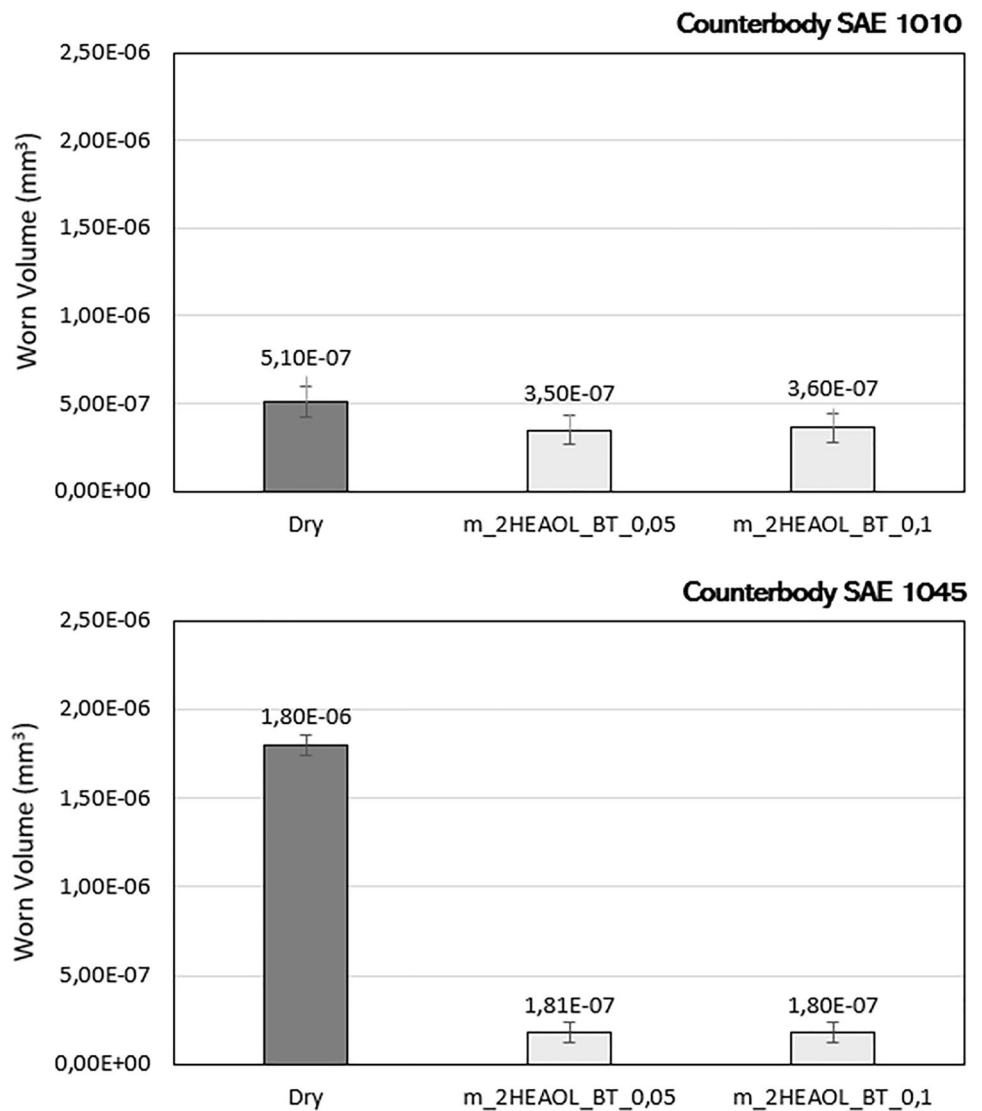
This worn volume was approximately 100 × smaller than the other lubricated tests of both substrates. However, unlike the other lubricated tests, which formed oxides in islands along the wear tracks, showed marked wear, and were detected in islands along the track (Fig. 10), the formation of a thick and continuous oxide layer occurred along the entire wear track, in the case of AISI/SAE 1045 steel lubricated with m-2HEAOL_BT_0.1. Raman analysis predominantly detected the formation of magnetite (Fe_3O_4) in the oxide layer (Fig. 10).

3.4 Tribofilm Formation Mechanism

The electrochemical tests showed the corrosive effect of bentonite, mainly in the polarization curve of the Water_BT_0.1 electrolyte in the AISI/SAE 1045 steel. This corrosive effect was inhibited by m-2HEAOL, as seen in Fig. 2 and Table 4. It is known that the PIL establishes a mixed type of adsorption (physisorption + chemisorption), inhibiting the steel corrosive process [34]. The anionic part of the ionic liquid can be easily adsorbed at positively charged sites on the worn surface of the steel, forming a reaction film on the newly worn surface of the sample, inhibiting the corrosive process [61]. However, the thickness of the oxide formed on the AISI/SAE 1045 steel in the m-2HEAOL_BT_0.1 test could indicate that the electrochemical effect was present during this wear test. In this case, the corrosion capacity of the bentonite was present due to the exposure of the substrate in the wear track and due to the disturbance of the adsorbed layer of the m-2HEAOL lubricant by the counterbody, accelerating the growth of the oxide layer formed mainly by magnetite (Fe_3O_4), the main oxide formed in the regions of interaction between steel and clay [10]. Thus, the use of a corrosion inhibitor that acts with an inhibition mechanism different from that of the PIL could impair the formation of the oxide film and increase the volume worn.
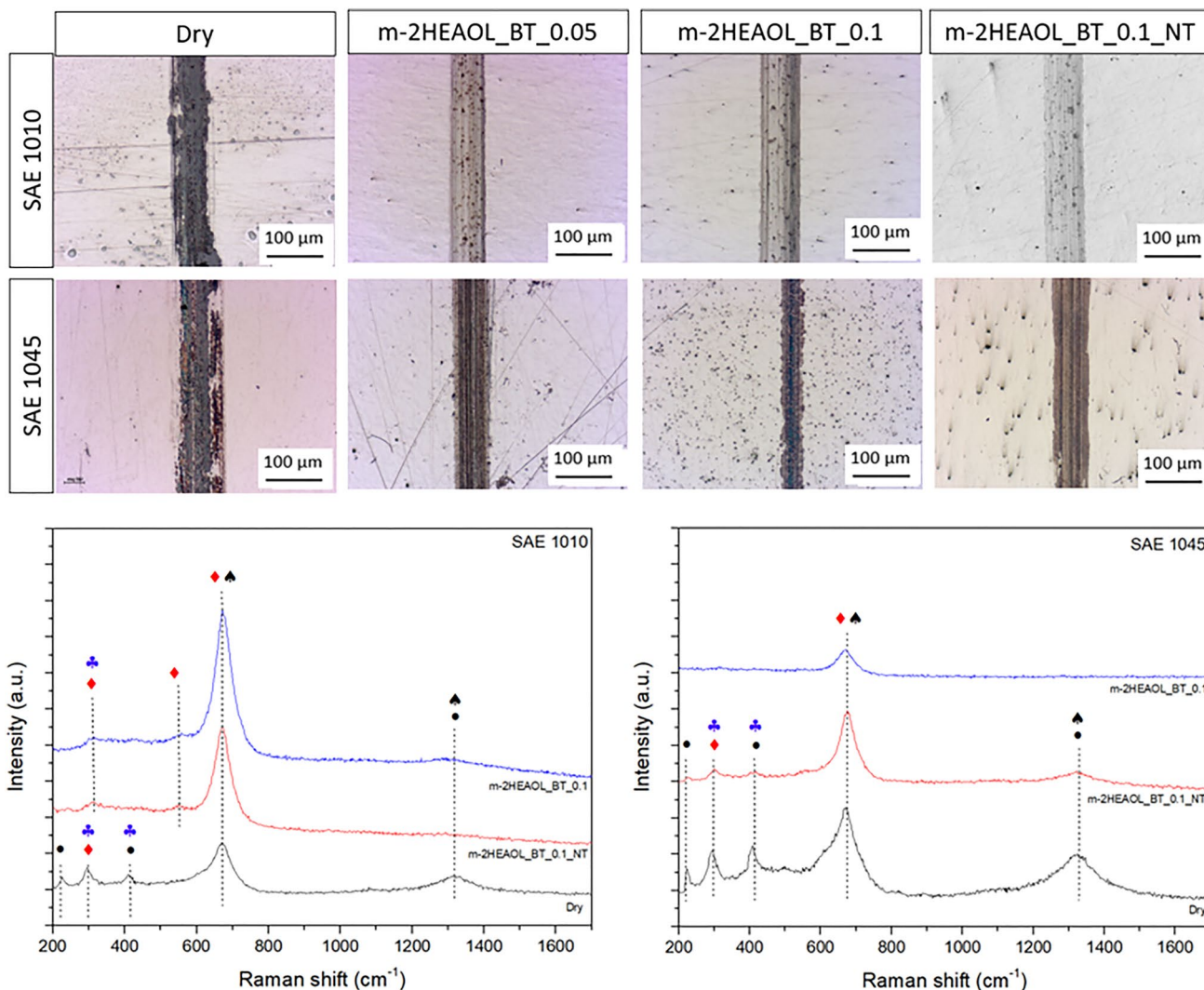
Fig. 10 Optical microscopy of wear tracks and RAMAN analysis (wavelength of 632.8 nm) on wear tracks. Where $\bullet = \alpha\text{-Fe}_2\text{O}_3$ (hematite), $\blacklozenge = \text{Fe}_3\text{O}_4$ (magnetite), $\clubsuit = \alpha\text{-FeOOH}$ (goetite), $\spadesuit = \gamma\text{-FeOOH}$ (lepidocricite)

The $NaNO_2$(sodium nitrite) is an anodic oxidizing corrosion inhibitor that contributes to the elevation of the corrosion potential of Fe and induces the formation of passivating Fe oxides, such as Fe_3O_4 e $\gamma - Fe_2O_3$ [75, 76]. In this context, tests were carried out on the m-2HEAOL_BT_0.1_NT formulation, which contained 1000 ppm of $NaNO_2$.

Figure 11 shows that the cross-sectional profile of the track lubricated with m-2HEAOL_BT_0.1_NT presented a geometry very similar to the track formed in the test with this lubricant without m-2HEAOL_BT_0.1 nitrite in AISI/SAE 1010 steel. This is due to the lowest corrosivity of this material, as previously mentioned. As the volume worn on AISI/SAE 1010 steel with and without the presence of $NaNO_2$ in the formulation was similar (4.25×10^{-4} mm^3 and 4.35×10^{-4} mm^3, respectively), it can be deduced that sodium nitrite does not interfere with the lubricity

and the ability to form tribochemical oxides in this steel. However, the track profile in the m-2HEAOL_BT_0.1_NT formulation in the AISI/SAE 1045 steel presented a larger geometry than the same formulation without sodium nitrite. The measured worn volumes were 2.70×10^{-4} mm^3 and 1.14×10^{-6} mm^3, respectively. Therefore, the corrosion inhibition capacity by steel passivation carried out by, contributed to the decrease in the thickness of the Fe oxide formed, preventing the protective effect against the wear of this high hardness layer, increasing the worn volume. Thus, the electrochemical effect of bentonite on the positively charged metal of the surface of the track during the tribological process contributed to the thickening of the oxide film formed in the m-2HEAOL_BT_0.1 formulation in the AISI/SAE 1045 steel, which had the most susceptible microstructure to corrosion.
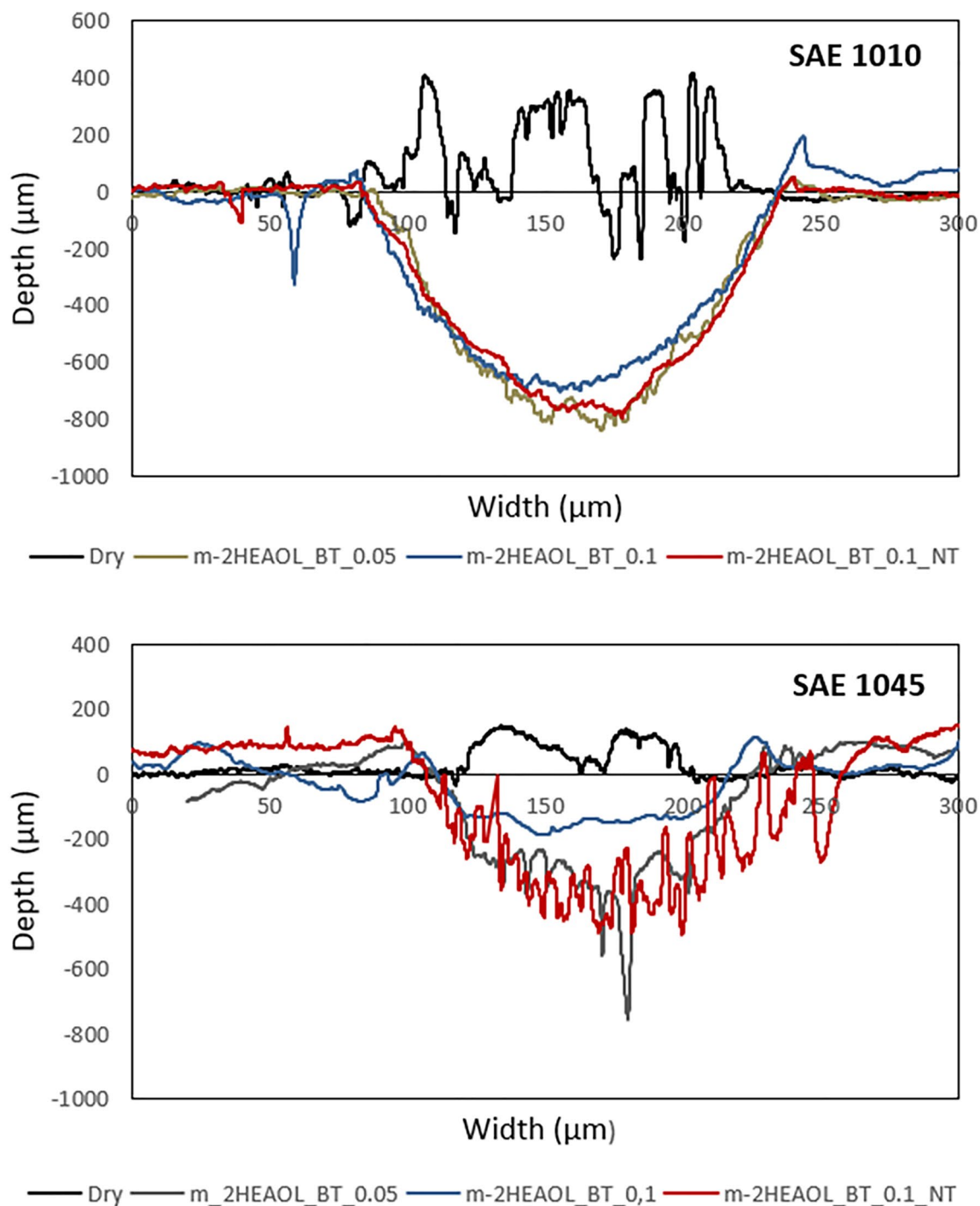
Fig. 11 Cross section of wear tracks and worn volume of steel samples

This layer is formed according to the mechanism described by Gaudin et. al. [10] and in item 3.2. However, the wear process in the track makes its surface more corrosion activated, resulting in a synergistic effect between wear and surface oxidation, increasing the oxide film thickness. Furthermore, the thermal effect generated by friction during the wear test may also have contributed to the thickening of the oxide film (trioxidation) [71]. These mixed tribochemical reactions (triboxidation and tribocorrosion) probably occurred in all formulations on both substrates, forming hematite and magnetite (Fig. 10).

However, this homogeneous oxide layer did not form in the m-2HEAOL_BT_0.05 formulation. Therefore, the concentration of bentonite particles is a critical factor for the
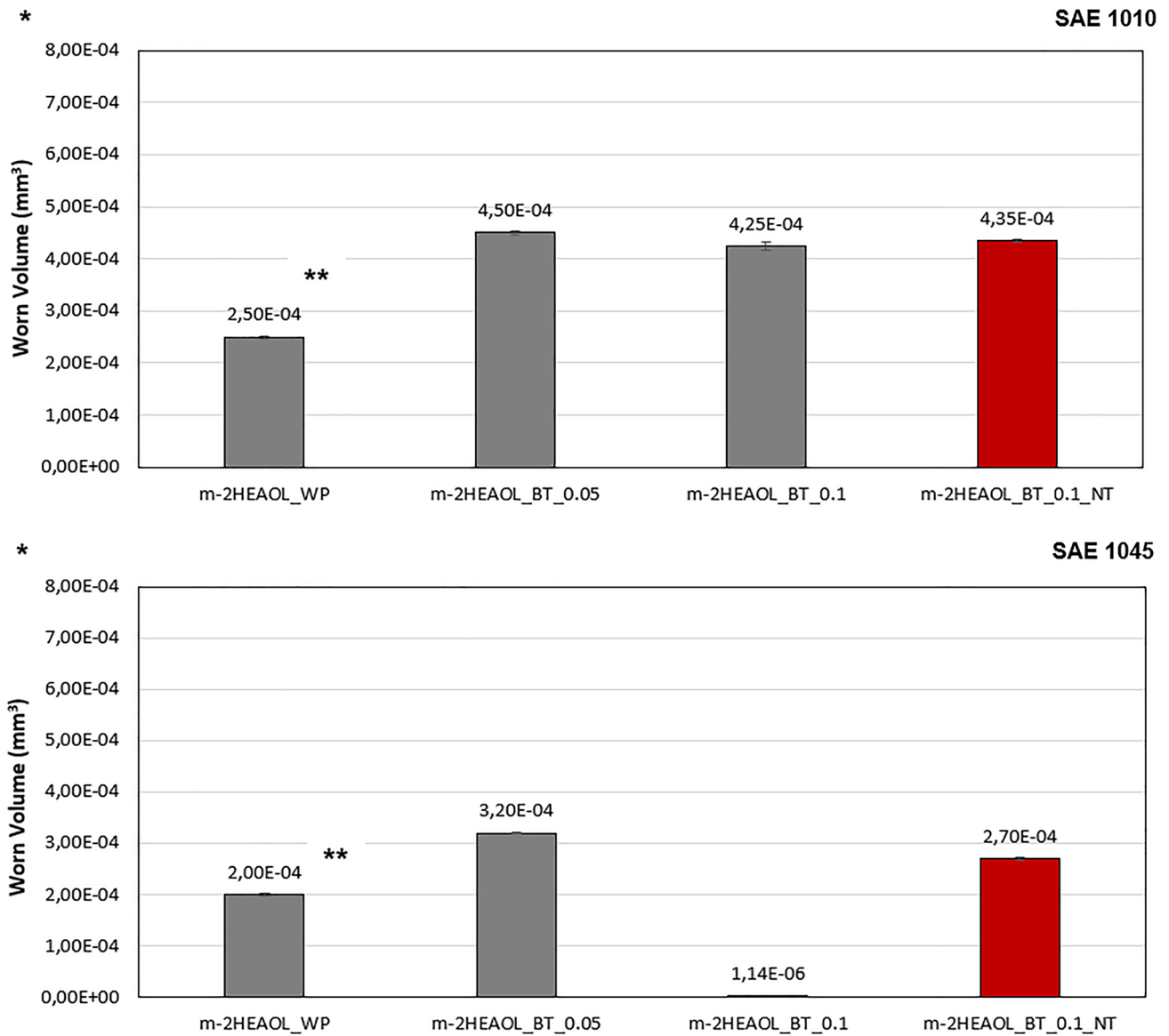
Fig. 12 Worn volumes of samples from both substrates. *It was not possible to detect the worn volume of the dry test; **Adapted from de Castro et al. [33]

Table 4 Electrochemical results obtained from the Tafel extrapolation

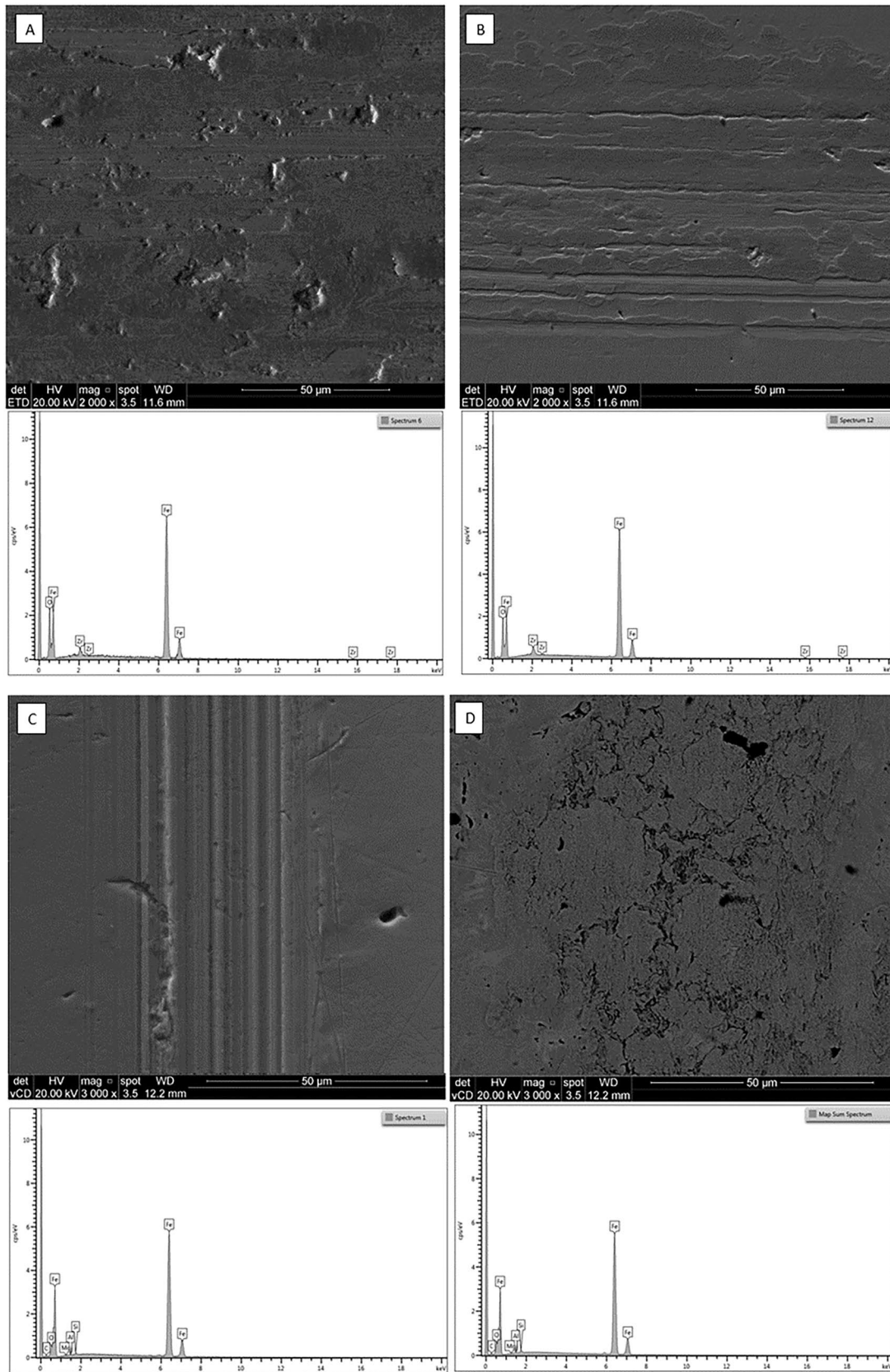| Lubricant	Substrate	Average E_{corr} (mV)	Average i_{cor} $[10^{-2}]$ (μA/cm^2)	CR $[10^{-4}]$ (mm/year)
Water_WP	SAE 1010	− 230 (29.0)	3.15 (0.7)	3.7
Water_BT_0.1		− 337.5 (32.0)	3.6 (0.8)	4.2
m-2HEAOL_WP		− 155 (7.0)	2.5 (0.7)	2.9
m-2HEAOL_BT_0.1		− 145 (35.0)	2.50 (0.7)	2.91
Water_WP	SAE 1045	− 305 (21.0)	17.5 (0.5)	20.4
Water_BT_0.1		− 462.5 (3.0)	100.0 (21.0)	116.5
m-2HEAOL_WP		− 225 (21.0)	13.5 (0.7)	15.8
m-2HEAOL_BT		− 180 (70.0)	29.3 (3.0)	34.20

Fig. 13 SEM/EDS analysis of wear tracks. **A** Lubrication-free wear track of SAE 1010 steel; **B** lubrication-free wear track of AISI/SAE 10 steel 10; **C** m-2HEAOL_BT_0.1-lubricated wear track of AISI/SAE 10 steel 45; **D** wear track lubricated with m-2HEAOL_BT_0.1 on AISI/SAE 1045 steel

occurrence of this phenomenon. Thus, the oxide layers did not reach the critical thickness and were removed during the wear test [69], leaving the oxide islands formed in the last moments of the wear tests. It should be noted that except for the tests carried out in the m-2HEAOL_BT_0.1 formulation on AISI/SAE 1045 steel, the eroded volumes found were higher than the formulation without particles, demonstrating the dominant role of the adsorbed film of m-2HEAOL in the lubricity of the formulations.

Apart from the film formation on AISI/SAE 1045 steel in the m-2HEAOL_BT_0.1 formulation, the percentage of bentonite studied did not contribute to improving the lubricity of lubricants containing PIL.

Unlike the behaviour found in lubricants with a commercial additive (Fig. 5), the bentonite particles addition, in the lubricant with the PIL, increased the worn volume of the wear tracks. Therefore, the lubricity provided by the adsorbed layer of PIL was predominant in the lubricity [33]. In addition, the presence of particles may have impaired the adsorbed layer, and this can be attributed to the oxides formed by tribochemical reaction, which did not reach the critical thickness and can be removed during the test [33]. In the case of m-2HEAOL_BT_0.1, the electrochemical effect evidenced in item 3.2 thickened the oxide film and drastically reduced the volume worn in quenched and tempered SAE 1045 steel, as previously mentioned.

It is noted that more active materials, such as quenched and tempered SAE 1045 steel, and on even more activated surfaces, such as within the wear tracks, facilitate the electrochemical performance of this clay, thickening the film through an electrochemical contribution.

Figure 13 shows the SEM/EDS analyses of wear tracks of dry and lubricated tests on both substrates. In the dry tests (Fig. 13A, B), for both substrates, in addition to the triboxidation generated by the tribochemical reaction mentioned above, groves are also observed in the direction of the sliding of the spheres, which is characteristic of microcutting/microplugging micromechanisms of abrasive wear [69, 77, 78], that is, abrasive wear occurred in the tests without lubrication despite the impossibility of measuring the worn volume. Craters were also detected, occurring mainly in the formed oxide layer. Probably the craters were generated by the propagation of cracks, possibly formed by the surface fatigue process [68].

The EDS analyses detected peaks of Zr arising from the wear process of the spheres mentioned above (Fig. 8), in addition to Fe and O, which are present in the oxide layers

and substrates. Figure 13C shows the test lubricated with m-2HEAOL_BT_0.1 of the AISI/SAE 1010 steel. The groves were predominantly detected, and they were generated by abrasive wear mode, more specifically by microcutting/microplugging sub-mechanisms. The m-2HEAOL_BT_0.1-lubricated AISI/SAE 1045 steel track (Fig. 13D) presents the oxide layer that significantly reduced wear in the test of this lubricant. The magnetite oxide formed prevented the existence of abrasive wear, and no grooves were found. Craters detected in the oxide layer suggest the occurrence of surface fatigue. EDS analyses did not detect signs of Zr in the lubricated test tracks, indicating that the lubricity of the tested formulations prevented the worn ball material from adhering to the wear tracks.

As demonstrated by the results presented, a thick oxide film formed during tribological testing of lubricant containing 0.1% (wt) bentonite on quenched and tempered SAE 1045 steel. This oxide prevented the evolution of the wear process and took the worn volume to values significantly lower than the tests in the other formulations (Fig. 9). There were some possibilities for the mechanism of formation of this oxide, such as thermal effects and tribochemical effects. The polarization curves confirmed the increase in the corrosivity of the formulations when adding bentonite particles. However, troboxidation generated by thermal effect, as occurred in the dry test, could be a possible formation mechanism. However, the RAMAN analysis of the oxide formed in the SAE 1045 steel test in the m-2HEAOL_BT_0.1 formulation was magnetite, which is formed in the corrosion process between clay and steel [10]. Furthermore, to confirm the corrosion mechanism hypothesis, a passivating corrosion inhibitor (sodium nitrite) was added, whose inhibition mechanism is different from m-2HEAOL. The formulation with inhibitor was called m-2HEAOL_BT_0.1_NT. Thus, in the test of this formulation in SAE 1045, it showed a higher eroded volume than the formulation without sodium nitrite, confirming the formation of this oxide in this tribological system. This formulation helped prove the electrochemical effect on the formation of this oxide during the wear tests.

4 Conclusions

In the present study, the effect of bentonite particles on water-based lubricants with a PIL was investigated. The tests aimed to evaluate the tribological and electrochemical performance of these lubricants. The main results are presented:

- The electrochemical tests showed that the bentonite particles contributed to the increase in the corrosion rates of the studied substrates, mainly in the quenched and tempered AISI/SAE 1045 steel.

- The formulations added with m-2HEAOL were able to mitigate the corrosive effect in the presence of water and these particles in the SAE 1010 steel.
- The m-2HEAOL inhibition mechanism (adsorption) was not able to mitigate the electrochemical effect of bentonite particles in the m-2HEAOL_BT_0.1 formulation in the SAE 1045, forming a layer of Fe oxide mainly constituted by magnetite (Fe_3O_4).
- The presence of oxide layer significantly reduced the worn volume in SAE 1045 steel.
- The inhibition power of $NaNO_2$ additive in the lubricating m-2HEAOL_BT_0.1_NT formulations was able to passivate the steel that favoured the increasing of the worn volume in the AISI/SAE 1045 steel test.
- The synergy between the corrosive effect of the particle and the tribological mechanisms in the wear track contributed to the thickening of the oxide film in the formulation without sodium nitrite inhibitor in the SAE 1045.
- Bentonite was able to mitigate the worn volume of wear tracks in formulations containing commercial additive.

Author Contributions VVdC: conceptualization; data curation; formal analysis; investigation; methodology; writing, review & editing; LMdS: data curation; formal analysis; investigation, review & editing; LMA: investigation; writing, review & editing; RMS: data curation; formal analysis; investigation; supervision; validation; review & editing; SM: supervision; review & editing; KSS: investigation, supervision; review & editing; MBP: investigation, supervision; review & editing; CRdLL: review & editing; SE: supervision; review & editing; CAdS: supervision; data curation; review & editing; CdFM: conceptualization; data curation; formal analysis; investigation; methodology; project administration; supervision; validation; visualization; review & editing.

Data availability Data will be made available on request.

Declarations

Competing interests The authors declare no competing interests.

Conflict of interest The authors declare that they have no conflict of interest.

Ethical Approval and Consent to Participate Not applicable.

Consent for Publication The author transfers to the concerned publisher the non-exclusive publication rights and the warrants that his contribution is original and that he has full power to make this grant. The author signs for and accepts responsibility for releasing this material on behalf of any and all co-authors. This transfer of publication rights covers the non-exclusive right to reproduce and distribute the article, including reprints, translations, photographic reproductions, microform, electronic form (offline, online), or any other reproductions of similar nature.

References

1. Rahman MH, Warneke H, Webbert H et al (2021) Water-based lubricants: development, properties, and performances. Lubricants 9:73. https://doi.org/10.3390/lubricants9080073
2. Rojas-Campanur M, Lara-Romero J, Chiñas-Castillo F, Alonso-Nuñez G (2007) Tribological performance of rosin acid additives in water based lubricants. Tribol Online 2:29–33. https://doi.org/10.2474/trol.2.29
3. Rodrigues AO, Angélica RS, Paz SPA (2021) DIFERENCIAÇÃO CATIÔNICA DE BENTONITAS POR INFRAVERMELHO: UM ESTUDO DOS EFEITOS DA HIDRATAÇÃO DOS CÁTIONS TROCÁVEIS. Quím Nova 44:272–277. https://doi.org/10.21577/0100-4042.20170705
4. Luz AB da, Lins FAF (2008) Rochas & minerais industriais: usos e especificações. CETEM/MCT
5. Namli M, Guler E (2017) Effect of bentonite slurry pressure on interface friction of pipe jacking. J Pipeline Syst Eng Pract 8:04016016. https://doi.org/10.1061/(ASCE)PS.1949-1204.0000255
6. Coelho ACV, de Santos PS, de Santos HS (2007) Argilas especiais: argilas quimicamente modificadas - uma revisão. Quím Nova 30:1282–1294. https://doi.org/10.1590/S0100-40422007000500042
7. Guillaume D (2002) Etude expérimentale du système fer-smectite en présence de solution à 80°C et 300°C. Université Henri Poincaré - Nancy, Phdthesis, p 1
8. Combarieu G de, Minet Y, Godon N, Barboux P (2005) Iron corrosion in Callovo-Oxfordian argilite
9. de Combarieu G, Barboux P, Minet Y (2007) Iron corrosion in callovo-oxfordian argilite: from experiments to thermodynamic/kinetic modelling. Phys Chem Earth Parts A/B/C 32:346–358. https://doi.org/10.1016/j.pce.2006.04.019
10. Gaudin A, Gaboreau S, Tinseau E et al (2009) Mineralogical reactions in the *Tournemire argillite* after in-situ interaction with steels. Appl Clay Sci 43:196–207. https://doi.org/10.1016/j.clay.2008.08.007
11. Khan A, Gusain R, Sahai M, Khatri OP (2019) Fatty acids-derived protic ionic liquids as lubricant additive to synthetic lube base oil for enhancement of tribological properties. J Mol Liq 293:111444. https://doi.org/10.1016/j.molliq.2019.111444
12. Galiński M, Lewandowski A, Stępniak I (2006) Ionic liquids as electrolytes. Electrochim Acta 51:5567–5580. https://doi.org/10.1016/j.electacta.2006.03.016
13. Egorova KS, Gordeev EG, Ananikov VP (2017) Biological activity of ionic liquids and their application in pharmaceutics and medicine. Chem Rev 117:7132–7189. https://doi.org/10.1021/acs.chemrev.6b00562
14. Liu H, Yu H (2019) Ionic liquids for electrochemical energy storage devices applications. J Mater Sci Technol 35:674–686. https://doi.org/10.1016/j.jmst.2018.10.007

15. Armand M, Endres F, MacFarlane DR et al (2009) Ionic-liquid materials for the electrochemical challenges of the future. Nat Mater 8:621–629. https://doi.org/10.1038/nmat2448

16. Ye C, Liu W, Chen Y, Yu L (2001) Room-temperature ionic liquids: a novel versatile lubricant. Chem Commun. https://doi.org/10.1039/B106935G

17. Pejaković V, Kronberger M, Mahrova M et al (2012) Pyrrolidinium sulfate and ammonium sulfate ionic liquids as lubricant additives for steel/steel contact lubrication. Proc Inst Mech Eng Part J 226:923–932. https://doi.org/10.1177/1350650112448978

18. Del Sol I, Gámez AJ, Rivero A, Iglesias P (2019) Tribological performance of ionic liquids as additives of water-based cutting fluids. Wear 426–427:845–852. https://doi.org/10.1016/j.wear.2019.01.109

19. Guo H, Iglesias P (2021) Tribological behavior of ammonium-based protic ionic liquid as lubricant additive. Friction 9:169–178. https://doi.org/10.1007/s40544-020-0378-z

20. Duan Z, Gu Y, Zhang J et al (2006) Protic pyridinium ionic liquids: synthesis, acidity determination and their performances for acid catalysis. J Mol Catal A 250:163–168. https://doi.org/10.1016/j.molcata.2006.01.035

21. Madankar CS, Pradhan S, Naik SN (2013) Parametric study of reactive extraction of castor seed (*Ricinus communis* L.) for methyl ester production and its potential use as bio lubricant. Ind Crops Prod 43:283–290. https://doi.org/10.1016/j.indcrop.2012.07.010

22. Greaves TL, Drummond CJ (2008) Protic ionic liquids: properties and applications. Chem Rev 108:206–237. https://doi.org/10.1021/cr068040u

23. Chen H, Cai T, Li H et al (2023) Macroscale superlubricity of steel by polymer-based ionic liquids without a running-in period. Tribol Int 182:8349. https://doi.org/10.1016/j.triboint.2023.108349

24. Kreivaitis R, Gumbytė M, Kupčinskas A et al (2023) Tribological properties of protic ionic liquid as an additive in aqueous glycerol solution for ruby-bearing steel tribo-contact. Lubricants 11:34. https://doi.org/10.3390/lubricants11010034

25. Donato MT, Deuermeier J, Colaço R et al (2023) New protic ionic liquids as potential additives to lubricate Si-based MEMS/NEMS. Molecules 28:2678. https://doi.org/10.3390/molecules28062678

26. Ortega Vega MR, Ercolani J, Mattedi S et al (2018) Oleate-based protic ionic liquids as lubricants for aluminum 1100. Ind Eng Chem Res 57:12386–12396. https://doi.org/10.1021/acs.iecr.8b02426

27. Saurín N, Avilés MD, Espinosa T et al (2017) Carbon nanophases in ordered nanofluid lubricants. Wear 376–377:747–755. https://doi.org/10.1016/j.wear.2017.01.008

28. Pamies R, Avilés MD, Arias-Pardilla J et al (2018) Antiwear performance of ionic liquid+graphene dispersions with anomalous viscosity-temperature behavior. Tribol Int 122:200–209. https://doi.org/10.1016/j.triboint.2018.02.020

29. Zhang L, Pu J, Wang L, Xue Q (2014) Frictional dependence of graphene and carbon nanotube in diamond-like carbon/ionic liquids hybrid films in vacuum. Carbon 80:734–745. https://doi.org/10.1016/j.carbon.2014.09.022

30. Avilés MD, Carrión-Vilches FJ, Sanes J, Bermúdez MD (2019) Diprotic ammonium succinate ionic liquid in thin film aqueous lubrication and in graphene nanolubricant. Tribol Lett 67:26. https://doi.org/10.1007/s11249-019-1138-y

31. Arcifa A, Rossi A, Ramakrishna SN et al (2018) Lubrication of Si-based tribopairs with a hydrophobic ionic liquid: the multiscale influence of water. J Phys Chem C 122:7331–7343. https://doi.org/10.1021/acs.jpcc.8b01671

32. Espinosa T, Jiménez M, Sanes J et al (2014) Ultra-low friction with a protic ionic liquid boundary film at the water-lubricated sapphire-stainless steel interface. Tribol Lett 53:1–9. https://doi.org/10.1007/s11249-013-0238-3

33. de Castro VV, dos Santos LM, Antonini LM et al (2023) Water-based lubricant containing protic ionic liquids and talc lubricant particles: Wear and corrosion analysis. Wear. https://doi.org/10.1016/j.wear.2023.204633

34. Schmitzhaus TE, Ortega Vega MR, Schroeder R, et al (2020) An amino-based protic ionic liquid as a corrosion inhibitor of mild steel in aqueous chloride solutions. Mater Corros maco.201911347. https://doi.org/10.1002/maco.201911347

35. Schmitzhaus TE, Ortega Vega MR, Schroeder R et al (2020) N-methyl-2-hydroxyethylammonium oleate ionic liquid performance as corrosion inhibitor for mild steel in hydrochloric acid medium. Mater Corros 71:1885–1902. https://doi.org/10.1002/maco.202011709

36. Schmitzhaus TE, Vega MRO, Schroeder R et al (2022) Localized corrosion behavior studies by SVET of 1010 steel in different concentrations of sodium chloride containing [m-2HEA][Ol] ionic liquid as corrosion inhibitor. Electrochim Acta 419:140385

37. Ortega Vega MR, Baldin EK, Pereira DP et al (2021) Toxicity of oleate-based amino protic ionic liquids towards *Escherichia coli*, Danio rerio embryos and human skin cells. J Hazard Mater. https://doi.org/10.1016/j.jhazmat.2021.126896

38. Iglesias M, Gonzalez-Olmos R, Cota I, Medina F (2010) Brønsted ionic liquids: Study of physico-chemical properties and catalytic activity in aldol condensations. Chem Eng J 162:802–808. https://doi.org/10.1016/j.cej.2010.06.008

39. Mattedi S, Carvalho PJ, Coutinho JAP et al (2011) High pressure CO_2 solubility in N-methyl-2-hydroxyethylammonium protic ionic liquids. J Supercrit Fluids 56:224–230. https://doi.org/10.1016/j.supflu.2010.10.043

40. ASTM G102 (1994) ASTM G102-89(2015)e1 Standard Practice for Calculation of Corrosion Rates and Related Information from Electrochemical Measurements. https://www.astm.org/Standards/G102. Accessed 8 Nov 2021

41. ASTM G133 (2016) Test method for linearly reciprocating ball-on-flat sliding wear. ASTM International, Washington, DC

42. Nakayama K, Martin J-M (2006) Tribochemical reactions at and in the vicinity of a sliding contact. Wear 261:235–240. https://doi.org/10.1016/j.wear.2005.10.012

43. Guo H, Smith T, Iglesias P (2019) The study of hexanoate-based protic ionic liquids used as lubricants in steel-steel contact. J Mol Liq. https://doi.org/10.1016/j.molliq.2019.112208

44. Qu J, Blau PJ, Dai S et al (2009) Ionic liquids as novel lubricants and additives for diesel engine applications. Tribol Lett 35:181–189. https://doi.org/10.1007/s11249-009-9447-1

45. Tang Z, Li S (2014) A review of recent developments of friction modifiers for liquid lubricants (2007–present). Curr Opin Solid State Mater Sci 18:119–139. https://doi.org/10.1016/j.cossms.2014.02.002

46. Spikes HA (2002) Film-forming additives—direct and indirect ways to reduce friction. Lubr Sci 14:147–167. https://doi.org/10.1002/ls.3010140204

47. BaruelI AF, DutraI RCL, Baldan MR et al (2018) Organofilização e silanização de argila bentonita. Quim Nova 41:134–139. https://doi.org/10.21577/0100-4042.20170160

48. Garnica AIC, da Curbelo FDS, Magalhães RR, de Sousa RPF (2018) EFEITOS DE SURFACTANTES NA ORGANOFILIZAÇÃO DE ARGILAS BENTONÍTICAS PARA USO EM FLUIDOS DE PERFURAÇÃO DE BASE MICROEMULSIONADA. HOLOS 4:89–105. https://doi.org/10.15628/holos.2018.7089

49. Bertuol K (2020) Estudo do efeito sinérgico cavitação/erosão em revestimentos de carboneto de cromo e tungstênio depositados por aspersão térmica de alta velocidade. Study of synergistic cavitation/erosion effect on chromium and tungsten carbide coatings deposited by high velocity oxy-fuel

50. Cavalcante M da S, Angélica RS (2014) Organofilização de uma Mg-bentonita da bacia do Parnaíba-Sul do Maranhão e sua utilização em poli (metacrilato de metila)

51. Álvarez VH, Mattedi S, Martin-Pastor M et al (2010) Synthesis and thermophysical properties of two new protic long-chain ionic liquids with the oleate anion. Fluid Phase Equilib 299:42–50. https://doi.org/10.1016/j.fluid.2010.08.022

52. Katiyar PK, Misra S, Mondal K (2019) Comparative corrosion behavior of five microstructures (pearlite, bainite, spheroidized, martensite, and tempered martensite) made from a high carbon steel. Metall Mater Trans A 50:1489–1501. https://doi.org/10.1007/s11661-018-5086-1

53. Clover D, Kinsella B, Pejcic B, De Marco R (2005) The influence of microstructure on the corrosion rate of various carbon steels. J Appl Electrochem 35:139–149. https://doi.org/10.1007/s10800-004-6207-7

54. Jeannin M, Calonnec D, Sabot R, Refait Ph (2010) Role of a clay sediment deposit on the corrosion of carbon steel in 0.5molL^{-1} NaCl solutions. Corros Sci 52:2026–2034. https://doi.org/10.1016/j.corsci.2010.02.033

55. Golubev SV, Bauer A, Pokrovsky OS (2006) Effect of pH and organic ligands on the kinetics of smectite dissolution at 25°C. Geochim Cosmochim Acta 70:4436–4451. https://doi.org/10.1016/j.gca.2006.06.1557

56. Akbulut M (2012) Nanoparticle-based lubrication systems. J Powder Metall Min. https://doi.org/10.4172/2168-9806.1000e101

57. Xiao H, Guo D, Liu S et al (2011) Film thickness of ionic liquids under high contact pressures as a function of alkyl chain length. Tribol Lett 41:471–477. https://doi.org/10.1007/s11249-010-9729-7

58. Wu J, Luo Y, Chen Y et al (2022) Poly(ionic liquid)s as lubricant additives with insight into adsorption-lubrication relationship. Tribol Int 165:107278. https://doi.org/10.1016/j.triboint.2021.107278

59. Kondo H (2008) Protic ionic liquids with ammonium salts as lubricants for magnetic thin film media. Tribol Lett 31:211–218. https://doi.org/10.1007/s11249-008-9355-9

60. Huang G, Yu Q, Ma Z et al (2017) Probing the lubricating mechanism of oil-soluble ionic liquids additives. Tribol Int 107:152–162. https://doi.org/10.1016/j.triboint.2016.08.027

61. Liu X, Zhou F, Liang Y, Liu W (2006) Tribological performance of phosphonium based ionic liquids for an aluminum-on-steel system and opinions on lubrication mechanism. Wear 261:1174–1179. https://doi.org/10.1016/j.wear.2006.03.018

62. Miyajima M, Matsumoto K, Kitamura K (2017) Characterization of Tribochemical Reactions on Steel Surfaces. 7

63. Hsu SM, Zhang J, Yin Z (2002) The nature and origin of tribochemistry. Tribol Lett 13:131–139. https://doi.org/10.1023/A:1020112901674

64. Rigney DA, Chen LH, Naylor MGS, Rosenfield AR (1984) Wear processes in sliding systems. Wear 100:195–219. https://doi.org/10.1016/0043-1648(84)90013-9

65. Reddy AS, Bai BNP, Murthy KSS, Biswas SK (1994) Wear and seizure of binary Al-Si alloys. Wear 171:115–127. https://doi.org/10.1016/0043-1648(94)90354-9

66. Crockett RM, Derendinger MP, Hug PL, Roos S (2004) Wear and electrical resistance on diesel lubricated surfaces undergoing reciprocating sliding. Tribol Lett 16:187–194. https://doi.org/10.1023/B:TRIL.0000009729.15103.5c

67. Guo H, Lou C, Pang J et al (2022) Linear alkyl-benzenesulfonate-based protic ionic liquids: physicochemical properties and tribological performance as lubricant additives to a non-polar base oil. J Mol Liq 361:119535. https://doi.org/10.1016/j.molliq.2022.119535

68. Stemmer P, Fischer A (2018) Pathways of dissipation of frictional energy under boundary lubricated sliding wear of martensitic materials. Lubricants 6:34. https://doi.org/10.3390/lubricants6020034

69. Heinz K, Gahr Z (1987) Microstructure and wear of materials, 1st edn. Elsevier, Amsterdam

70. Quinn TFJ (1983) NASA interdisciplinary collaboration in tribology, vol 118

71. Quinn TFJ, Sullivan JL, Rowson DM (1984) Origins and development of oxidational wear at low ambient temperatures. Wear 94:175–191. https://doi.org/10.1016/0043-1648(84)90053-X

72. Batchelor AW, Stachowiak GW, Cameron A (1986) The relationship between oxide films and the wear of steels. Wear 113:203–223. https://doi.org/10.1016/0043-1648(86)90121-3

73. Basile LJ, Ferraro JR, Mitchell ML, Sullivan JC (1978) The raman scattering of actinide (VI) ions in carbonate media. Appl Spectrosc 32:535–537

74. Mäntyranta A, Heino V, Isotahdon E et al (2019) Tribocorrosion behaviour of two low-alloy steel grades in simulated waste solution. Tribol Int 138:250–262. https://doi.org/10.1016/j.triboint.2019.05.032

75. Hayyan M, Sameh SA, Hayyan A, AlNashef IM (2012) Utilizing of sodium nitrite as inhibitor for protection of carbon steel in salt solution. Int J Electrochem Sci 7:10

76. Wachter A (1945) Sodium nitrite as corrosion inhibitor for water. Ind Eng Chem 37:749–751. https://doi.org/10.1021/ie50428a021

77. de Castro VV, Mazzini Fontoura LA, Benfica JD et al (2016) Lubricated sliding wear of SAE 1045 and SAE 52100 steel against alumina in the presence of biodiesel, diesel and a 50:50 blend of those fuels. Wear 368–369:267–277. https://doi.org/10.1016/j.wear.2016.09.026

78. Xing S, Yu S, Deng Y et al (2012) Effect of cerium on abrasive wear behaviour of hardfacing alloy. J Rare Earths 30:69–73. https://doi.org/10.1016/S1002-0721(10)60641-2